PHILOSOPHICAL TRANSACTIONS OF THE ROYAL SOCIETY A MATHEMATICAL, PHYSICAL & ENGINEERING SCIENCES

Archetypal Response Patterns for Open Chemical Systems with Two Components

P. Gray and S. K. Scott

Phil. Trans. R. Soc. Lond. A 1990 **332**, 69-87
doi: 10.1098/rsta.1990.0101

Archetypal response patterns for open chemical systems with two components

By P. Gray[1] and S. K. Scott[2]

[1] *Gonville and Caius College, Cambridge CB2 1TA, U.K.*

[2] *School of Chemistry, University of Leeds, Leeds LS2 9JT, U.K.*

The dynamics of nonlinear, dissipative systems have become a centre of interest in many fields. Autocatalysis, whether encountered in biochemistry, chemical engineering, chemistry or combustion, offers a perplexing variety of nonlinear behaviour which is gradually being codified. Archetypal model systems simple enough to be analysed deeply (or computed informatively) are of the greatest value not only in revealing how little is needed to generate great variety in behaviour, but also in understanding exactly how it arises. We consider here the simplest of open systems (CSTR) and see how far the isothermal scheme: $A + 2B \rightarrow 3B$; $B \rightarrow C$ goes to explaining the existence of alternative oscillatory patterns in the oxygen–hydrogen reaction.

1. Introduction

When chemical reactions occur in open systems – and in the natural world even more than in chemical industry the open system is the prevalent mode – stationary states and sustained oscillations may be realized. It is also possible to encounter multiple stationary states and to observe discontinuous jumps between them or from steady states to oscillatory behaviour. In closed systems, in which chemical change ends with a state of chemical equilibrium, truly stationary intermediate states are not found although the invaluable approximation – originally due to Bodenstein – called the 'stationary-state hypothesis' is a very familiar one. Investigations of oscillatory chemical systems have gone through phases. First, closed systems were almost the only ones studied: batch processes. In solution chemistry, in the late 1970s it was still necessary to plead (Gray 1980) for more studies of open systems. The well-stirred reactor with continuous inflow and outflow (CSTR) then became more popular, not least because so many systems seemed to show oscillatory instabilities in these circumstances. The pendulum swung a long way. The experimental care necessary to generate really adequate spatial uniformity did not always match the enthusiasm of the investigators, and the catch phrase 'far from equilibrium' was sometimes less significant than 'far from homogeneity'. These circumstances make the study of idealized models of great importance, especially if they are easily manipulated mathematically and chemically self-consistent. They allow us not only to realize that very simple overall chemical properties can give rise to the most varied behaviour, but also to test models for imperfect mixing and to predict the effect of irremoveable fluctuations and imperfect experimental control.

Work of this nature in simple chemical systems exhibiting thermal feedback goes back to Zel'dovich in 1941 (stationary states) and Sal'nikov in 1948 (oscillations):

Phil. Trans. R. Soc. Lond. A (1990), **332**, 69–87 *Printed in Great Britain*

the modern era was ushered in by Amundson (1955, 1958) and Aris (1958). There the nonlinearities are strong (approximately exponential in excess temperature) and the intensity of feedback in gaseous systems as measured by the Zel'dovich number is large. In isothermal circumstances chemical autocatalysis or autoinhibition offers a feedback mechanism and it is to autocatalysis in the CSTR that we turn in this article. An astonishing richness in behaviour is revealed and attention is drawn to recent work in birhythmicity in the oxygen–hydrogen reaction.

2. Model scheme and reaction rate equations

The basic requirements for 'exotic' behaviour such as oscillations or multistability are that the reaction should have some mechanism for feedback and that the reaction rate equations should have a sufficiently high dependence of rate on concentrations (they should be sufficiently nonlinear). The simplest chemical model that satisfies these is that of cubic autocatalysis. Such a process, whereby a given species catalyses its own production can be compactly represented as

$$\mathrm{A}+2\mathrm{B}\rightarrow 3\mathrm{B} \quad \text{rate} = k_1 ab^2. \tag{1}$$

Here A is the reactant and B the autocatalyst: the rate of this step is overall third order in concentration. The implications of such a representation for the underlying chemical mechanism have been widely discussed elsewhere (Aris *et al.* 1988; Cook *et al.* 1989; Gray & Scott 1989; Kaas-Petersen *et al.* 1989): here we simply remark that it is not necessary to believe this is a single, termolecular elementary step but rather may be an empirical rate-law for a suitable subscheme of, say, bimolecular reactions.

Reaction (1) alone can produce multiple stationary-state solutions in a well-stirred flow reactor, but not oscillations. The latter will require at least two independent concentrations. Although reaction (1) involves two chemical species, their concentrations are not independent but instead are related by the stoichiometric conservation condition $a+b=$ const. at all times. To decouple these concentrations we can simply introduce a second reaction and for this we choose the first-order decay of the autocatalyst to a final product C:

$$\mathrm{B}\rightarrow\mathrm{C} \quad \text{rate} = k_2 b. \tag{2}$$

Now stoichiometry requires $a+b+c=$ const. so two of the concentrations can vary independently.

(a) *Governing rate-equations for cubic autocatalysis in a* CSTR

We now imagine reactions (1) and (2) occurring in a well-stirred flow reactor fed by inflows of reactant A and autocatalyst B. The governing reaction rate of mass balance equations for the concentrations of these two species are

$$\mathrm{d}a/\mathrm{d}t = (a_0-a)/t_{\mathrm{res}} - k_1 ab^2 \tag{3}$$

and

$$\mathrm{d}b/\mathrm{d}t = \underset{\text{inflow–outflow}}{(b_0-b)/t_{\mathrm{res}}} + \underset{\text{chemical reaction}}{k_1 ab^2 - k_2 b}\ . \tag{4}$$

Here a_0 and b_0 are the concentrations that would be achieved in the CSTR after mixing of the inflow streams but in the absence of any reaction; t_{res} is the mean residence time and is given by the volume of the reactor divided by the total volumetric flow rate.

Equations (3) and (4) appear to offer five experimental parameters that might be varied: the inflow concentrations a_0 and b_0, the reaction-rate constants k_1 and k_2 and

the residence time. In fact, the qualitative behaviour of the system is not sensitive to the absolute values of these parameters, but rather to a smaller number of quotients formed from them. To show this, we should recast the equations in dimensionless form. The CSTR presents an obvious reference concentration relative to which others can be gauged: the inflow concentration of the reactant a_0. Thus we define the dimensionless concentrations

$$\alpha = a/a_0, \quad \beta = b/a_0 \quad \text{and} \quad \beta_0 = b_0/a_0. \tag{5}$$

With these forms we must then have $\alpha \leqslant 1$ as the concentration of A in the reactor cannot exceed that of the inflow and $\beta \leqslant 1+\beta_0$. The quantity β_0 is simply the relative inflow concentration of autocatalyst to reactant: usually we shall be interested in the situation $\beta_0 < 1$.

To measure timescales we use the chemical time t_{ch} formed from the autocatalytic reaction-rate constant: k_1 has implied units of concentration^{-2} s^{-1}; thus if we multiply this by the square of the reference concentration a_0^2 and then take the reciprocal we have

$$t_{\mathrm{ch}} = 1/k_1 a_0^2. \tag{6}$$

We can then define a dimensionless time τ, a dimensionless residence time τ_{res} and a dimensionless decay-rate constant κ_2 as

$$\tau = t/t_{\mathrm{ch}} = k_1 a_0^2 t, \quad \tau_{\mathrm{res}} = t_{\mathrm{res}}/t_{\mathrm{ch}} = k_1 a_0^2 t_{\mathrm{res}} \quad \text{and} \quad \kappa_2 = k_2 t_{\mathrm{ch}} = k_2/k_1 a_0^2. \tag{7}$$

With these dimensionless forms, the governing rate equations become

$$\mathrm{d}\alpha/\mathrm{d}\tau = (1-\alpha)/\tau_{\mathrm{res}} - \alpha\beta^2 \tag{8}$$

and

$$\mathrm{d}\beta/\mathrm{d}\tau = (\beta_0-\beta)/\tau_{\mathrm{res}} + \alpha\beta^2 - \kappa_2\beta. \tag{9}$$

In these terms, then, only three parameters appear explicitly: β_0, κ_2 and τ_{res}. It is also possible to make a further subdivision among these. The residence time is the parameter that can be most easily manipulated during a given experiment, by altering the pumping rate. On the other hand the relative inflow concentration β_0 and the dimensionless decay rate constant κ_2 would remain fixed during a given experiment although they might be varied between successive runs. Technically, we refer to τ_{res} as a bifurcation parameter with β_0 and κ_2 as unfolding parameters.

(*b*) *The parameter plane*

This distinction between the parameters also determines the philosophy through which we present our results. We consider how the behaviour of a system with particular, fixed values of β_0 and κ_2 varies with the dimensionless residence time, concentrating on qualitative features such as whether oscillations or multiple stationary states appear or disappear and how these would be observed experimentally. Next we wish to establish how these qualitative responses to τ_{res} depend on the unfolding parameters.

The details of the latter are presented elsewhere (Gray & Scott 1983, 1984, 1985*a*, *b*, 1989) and reviewed briefly here in the Appendix. The important features are summarized in figure 1, the $\beta_0-\kappa_2$ parameter plane. The various solid curves divide this plane into eight major regions, some of which are further subdivided by the broken curves. For all combinations of β_0 and κ_2 within any given region or subregion, the qualitative response of the system to varying the residence time is the same: the responses for parameter combinations from different regions are qualitatively distinct.

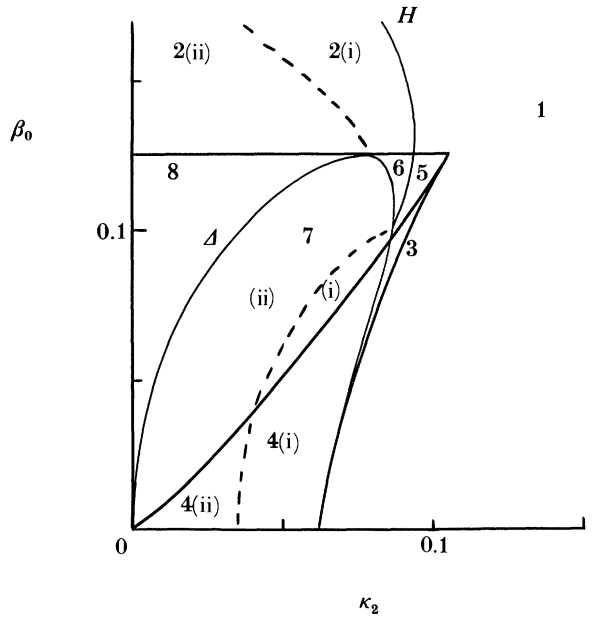

Figure 1. The regions of qualitatively different response in the $\beta_0-\kappa_2$ parameter plane. The boundaries represent loci of degenerate bifurcations (see Appendix).

(c) *Stationary states*

The typical behaviour of systems governed by rate equations of the form of (8) and (9) – or equivalently (3) and (4) – can frequently be deduced by considering first the potential stationary states. The latter are combinations of the concentrations $(\alpha_{ss}, \beta_{ss})$ for which both time derivatives become zero simultaneously. With the condition $d\alpha/d\tau = d\beta/d\tau = 0$ we have

$$\beta_{ss} = (1+\beta_0-\alpha_{ss})/(1+\kappa_2\tau_{res}) \tag{10}$$

and α_{ss} is given by the roots of a cubic equation

$$F(\alpha_{ss}, \tau_{res}:\beta_0, \kappa_2) = \frac{(1+\kappa_2\tau_{res})}{\tau_{res}}(1-\alpha_{ss})-\alpha_{ss}(1+\beta_0-\alpha_{ss})^2 = 0. \tag{11}$$

For positive values of the physical parameters τ_{res}, β_0 and κ_2 this equation always has at least one positive, real root, and may have three, corresponding to multiple stationary states. Gray & Scott (1983, 1984) give details of a graphical method for establishing the stationary-state behaviour of any given system and also of various special cases, such as that with no catalyst inflow $\beta_0 = 0$, for which the root $1-\alpha_{ss} = 0$ can be factored out of equation (11) leaving a quadratic so that all the roots are available in simple analytical forms.

3. Responses to dimensionless residence time

We now consider some of the possible 'bifurcation diagrams' for this model, corresponding to the qualitative changes in behaviour of a given system to varying the residence time, and how such changes determine the experimental observations.

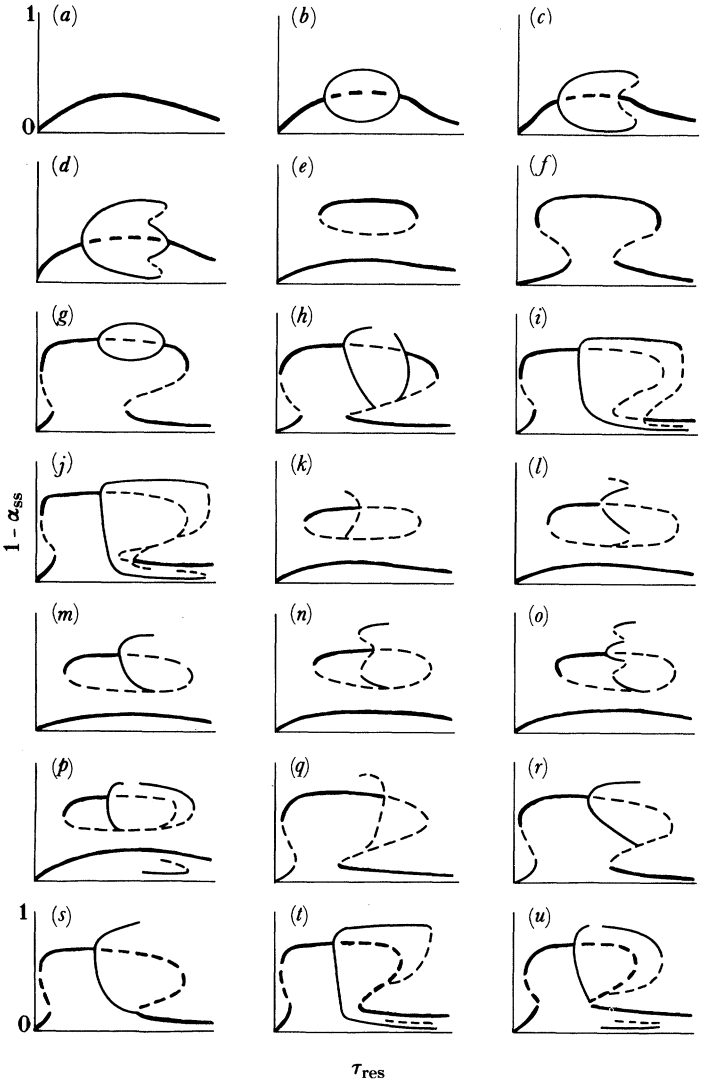

Figure 2. The 21 bifurcation diagrams for cubic autocatalysis with decay in a CSTR: solid thick lines, stable stationary states; broken thick lines, unstable stationary-states; solid thin lines, stable limit cycles; broken thin lines, unstable limit cycles.

For this we really need a three-dimensional picture, with some measure of the two concentrations forming two axes and the residence time as the third. Conventionally, however, we choose to present one projection and a series of sections through this space.

The projection shows the locus of stationary states for one of the concentrations as τ_{res} varies (but with β_0 and κ_2 still fixed) and may also indicate where oscillatory solutions exist. The choice here will be to plot the stationary-state 'extent-of-conversion', $1-\alpha_{ss}$, against τ_{res}. The sections are known as 'phase-portraits' and are slices through the three-dimensional picture at constant residence time. The stationary-state solutions given by equations (10) and (11) appear as points in the phase plane and time-dependent behaviour such as the approach to a given

stationary point is represented by motion across the plane, a 'trajectory' from some initial point. The use of these diagrams and their interpretation will become clearer with specific examples.

(*a*) *Region 1*

With relatively high values for the dimensionless inflow concentration of the autocatalyst β_0 and the decay rate constant κ_2, the system lies in region 1 of figure 1, to the right of and above the various boundary lines. The stationary-state locus for such parameter values is as shown in figure 2*a*: for any given residence time, the stationary-state condition (11) has one and only one real, positive root. There is a 'unique' stationary state for each residence time. Furthermore, the stationary state is always stable. The concept of stationary-state stability (local stability) will be of more importance in later examples and can be determined mathematically by the methods described in the Appendix. Physically, local stability implies that a small perturbation of the system away from the stationary state will decay with time: the system moves back to the same state.

The phase portrait appropriate to the present example is the same for all residence times. There is a single stationary point, as shown in figure 3*a*. If we start the system from any other point on the plane, the trajectory moves from the initial point to the stationary state as time increases: the stationary point is a stable sink. (It is also possible to classify further the sink as a node or a focus depending on whether the final approach is monotonic, or as a damped oscillation, but this distinction has less relevance away from the stationary point so is not discussed in much detail in this paper.)

(*b*) *Region 2*

With relative inflow concentrations of the two species such that $\frac{1}{8} < \beta_0 < 1$ and for more stable catalysts (so κ_2 is small), the system sits in region 2. The broken curve emanating from $\beta_0 = \frac{1}{8}$, $\kappa_2 = 3^4/4^5$ and approaching $\beta_0 = \frac{1}{3}$ as $\kappa_2 \to 0$ further distinguishes between subregions 2(i) and 2(ii).

Throughout region 2(i), the stationary-state bifurcation diagram has the form shown in figure 2*b*. There is again just one root of the stationary-state equation (11) for any given residence time and hence a unique singular point in any phase portrait. However, the stationary state is not always now stable. For a range of residence times, the stationary state is unstable: trajectories move away from the stationary point in the phase plane. This presents something of a problem: where does the system move to instead of going to the stationary state? Mass conservation tells us that at all times $(a+b) \leqslant (a_0+b_0)$, or $(\alpha+\beta) \leqslant (1+\beta_0)$ in dimensionless terms, and we also know that $1 \geqslant \alpha \geqslant 0$ and $\beta \geqslant 0$. Thus the system is constrained to remain within the quadrilateral region of the phase plane bordered by the two axes and by the lines $(1-\alpha) = 1$ and $\beta = (1-\alpha)+\beta_0$, as indicated in figure 4. We may also note that equation (10) requires all stationary-state solutions to lie on the same line in the phase plane. We may further restrict the motion of the trajectory on the plane: it cannot cross itself (except in some special sense at a singular point). If the trajectory were to cross itself, the gradient of the trajectory at that point would have to have two different values. However, the gradient, which is $\mathrm{d}\beta/\mathrm{d}(1-\alpha)$ is also given by $-(\mathrm{d}\beta/\mathrm{d}\tau)/(\mathrm{d}\alpha/\mathrm{d}\tau)$ and these two are given uniquely for specified values of α, β and the various parameters. Thus there can be only one gradient vector at any point in the phase plane and trajectories cannot cross.

What the trajectory can do is to join up, creating a closed loop. This is a limit cycle.

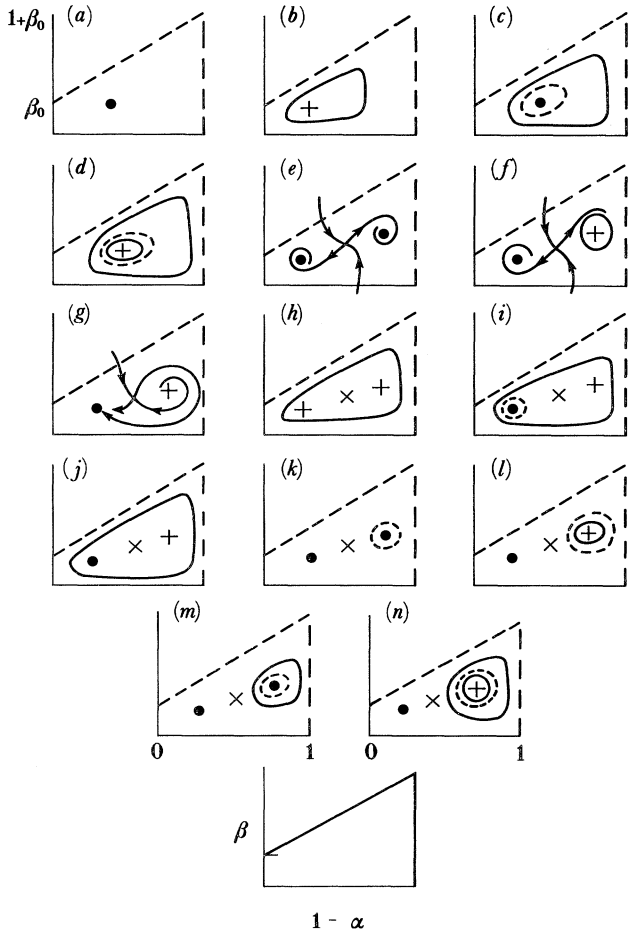

Figure 3. The 14 phase portraits for cubic autocatalysis with decay in a CSTR: ●, stable node or focus (sink); ×, saddle point; +, unstable node or focus (source): solid closed curves, stable limit cycle; broken closed curves, unstable limit cycle.

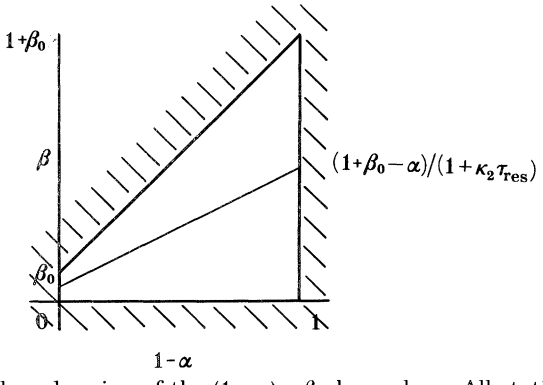

Figure 4. The allowed region of the $(1-\alpha)-\beta$ phase plane. All stationary-state solutions must lie on the line $\beta = (1+\beta_0-\alpha)/(1+\kappa_2\tau_{res})$.

Motion around such a (stable) limit cycle corresponds to sustained oscillations in the species concentrations occurring around the unstable stationary state. Figure 3*b* shows a phase portrait for an unstable stationary state surrounded by a stable limit cycle. The size of the limit cycle is related to the amplitude of the oscillations, given say by the difference between the maximum and minimum values of $(1-\alpha)$ attained during a circuit. The variation in size of the limit cycle with the residence time is indicated by plotting this maximum and minimum onto the locus in figure 2*b* around the unstable stationary state (indicated by a broken section of the locus).

The ends of the range of stationary-state instability are Hopf bifurcation points. Experimentally, if we start at low residence times, below the lower Hopf point, the system has a stable stationary state to which it moves. As the residence time is increased, the stationary state loses stability at the lower Hopf point and a stable limit cycle emerges in the phase-plane. At first, the limit cycle is vanishingly small, but it grows as we move away from the Hopf point. It cannot grow indefinitely: the system must stay within the allowed region of the phase plane. At some residence time, the limit cycle attains a maximum size and thereafter decreases again. As we approach the upper Hopf point, the limit cycle shrinks to zero size, converging onto the stationary-state point as this regains stability. In phase-plane terms we see the sequence 3(*a*)–3(*b*)–3(*a*) as the residence time is increased or if it is decreased.

In region 2(ii), the behaviour is slightly different. There is still only a single stationary state for any given residence time and this state loses its stability over the range between two points of Hopf bifurcation. However, the behaviour at the upper Hopf point is not the same as in region 2(i). The appropriate stationary-state bifurcation diagram is figure 2*c*. Starting from low residence time, there is a single, stable stationary point in the phase-plane (figure 3*a*). Increasing τ_{res} through the lower Hopf bifurcation, the stationary state loses stability and a stable limit cycle emerges, growing from zero amplitude (figure 3*b*). We refer to such Hopf points as supercritical bifurcations. The limit cycle grows in size attaining a flat, extended maximum as τ_{res} increases. The amplitude does not now decrease significantly as we approach the upper Hopf point from below. Instead a second limit cycle appears at the Hopf point. This is an unstable limit cycle and it emerges as the stationary state regains its stability. The growth of an unstable limit cycle around a stable stationary state characterizes a subcritical Hopf bifurcation.

Figure 3*c* shows the phase portrait just above the upper Hopf point. There are three coexisting features: the stable stationary point, the unstable limit cycle and the stable limit cycle. As two of these responses are stable, we cannot now say *a priori* what will be observed experimentally. If we have been sitting on the stable limit cycle at lower residence times, there is no reason why we should fall off just because the stationary state has become stable, so the system may continue to oscillate. In fact the unstable limit cycle plays an important role here. We cannot sit on an unstable cycle anymore than we can on an unstable stationary state: inevitable perturbations will disturb us and then grow. However, the unstable cycle separates the phase plane into two regions: one inside, the other outside that cycle. Any trajectory that starts from a point within the unstable limit cycle must remain within it (trajectories cannot cross themselves or each other) and so will be attracted to the stable stationary point. Initial conditions outside the unstable cycle will be attracted to the stable limit cycle. Steady and oscillatory states coexist.

As the residence time increases further, so the unstable cycle grows inside the stable one. Eventually, these two cycles can merge. Exactly at that point we

have a semi-stable limit cycle, but for any higher residence time the cycles have disappeared, annihilating each other. Now only a stable stationary point exists (figure 3*a*).

If we now begin to decrease the residence time, the stable and unstable limit cycles reappear, at the same value of τ_{res} at which they merged. However, the stationary state is still stable, so the system can remain there even though the stable limit cycle now exists again. Only at the Hopf point does the stationary state lose stability and the system move to the stable limit cycle. Thus we see hysteresis between the steady and oscillatory states. In this case, the stable limit cycle already has a finite size when the Hopf bifurcation occurs. The resulting oscillations thus begin with a non-zero amplitude. This is 'hard excitation'.

Finally, we may also note that in the region of hysteresis, the system can be moved from one stable response to another if a perturbation of sufficient magnitude is applied, to carry it across the unstable cycle in the phase plane.

One other response for some combinations in region 2, but for which the relevant sub-boundary has not been determined, is the possibility of three co-existing limit cycles: two stable and one unstable, surrounding an unstable stationary state. The appropriate stationary-state locus is shown in figure 2*d* and the extra phase portrait as figure 3*d*. Coexisting stable limit cycles lead to 'birhythmicity', with the possibility of large-amplitude or small-amplitude oscillations at the same parameter conditions, and hysteresis between these forms.

(*c*) *Regions 3 and 5*

The small regions close to the cusp in the parameter plane (figure 1) have similar behaviour to each other, with one qualitative difference. No oscillatory states are found, but there is now multiplicity of stationary states. In region 3, the stationary-state locus forms an 'isola' (figure 2*e*); in region 5 we have a 'mushroom' (figure 2*f*).

For the isola pattern there is a single stationary-state solution, corresponding to low extents of reaction, at the shortest residence times. In fact this branch of solutions exists and is locally stable for all residence times. The phase-portrait is as in figure 3*a*. As we increase τ_{res} two new branches of stationary states emerge. These form the lower and upper shores of the isola. These new states first appear as a saddle-node pair, i.e. a single point that separates into two. Above the saddle-node point, the system has two stable stationary states (the highest and lowest) and an unstable state (the middle one). The corresponding phase portrait is shown in figure 3*e*. All stationary points lie on the same line: the outer points are sinks, the middle is a saddle. Saddle points have two special pairs of trajectories as indicated in the figure. One pair approaches the saddle: these are the insets and they divide the phase plane in two, with one of the stable stationary states on each side. All other trajectories eventually leave the vicinity of the saddle point and do so tangent to the outset pair. The insets play the role of a separatrix: no trajectory may cross an inset, so those points starting on one side must move to the stable stationary state on that side, not the other.

As the residence time is increased further, the upper two solutions at first move apart; after some maximum separation, however, they move back towards each other again and eventually merge at a second saddle-node bifurcation point. For the highest residence times, only the low stationary state exists.

Provided we start on the lower branch, there is no reason why the system should move spontaneously away from that state, even though an alternative stable state

on the top of the isola may exist. We can persuade the system to change states in the region of multiplicity if we give it a sufficiently large perturbation. Once on the top of the isola, the system will remain there either until it receives another suitable, large perturbation or until the residence time is either increased or decreased beyond the saddle-node points. In the latter case we see 'extinction' or 'washout' from the state of high reaction. There is no spontaneous jump from low reaction to high, i.e. no 'ignition' for an isola. The progression of phase portraits is 3(*a*)–3(*e*)–3(*a*).

For a mushroom there is different behaviour at intermediate residence times. Now, the lower branch of stationary states merges with the saddle point branch. This creates two new saddle-node bifurcations, corresponding to ignition points: one ignition accompanies an increase in τ_{res}, the other a decrease. There are two regions of hysteresis between the ignition and extinction pairs. The lowest and highest stationary states are locally stable whenever they exist. The pattern of phase portraits now is 3(*a*)–3(*e*)–3(*a*)–3(*e*)–3(*a*), although we may note that the unique state in the middle of this sequence corresponds to high extents of conversion whereas those at the ends are low conversion states.

(*d*) *Regions 6 and 8*

Mushroom patterns are also found in regions 6 and 8 of the parameter plane (figure 1). Now multiplicity of stationary states is combined with the possibility of two Hopf bifurcation points and, hence, limit cycle solutions.

Region 6 lies between the lines H, Δ and $\beta_0 = \frac{1}{8}$. For such combinations of β_0 and κ_2 the mushroom has two supercritical Hopf bifurcations along its upper shore. A stable limit cycle emerges from each Hopf point, growing from zero amplitude as τ_{res} increases above the lower Hopf point or decreases below the upper. In the simplest case, these limit cycles are one and the same and meet up somewhere in the range of instability of the uppermost stationary state, as shown in figure 2*g*. This situation is favoured if the Hopf points also occur at lower residence times than the upper region of stationary-state hysteresis. If this is the case, there are no phase portraits other than those seen already. Increasing the residence time we follow the sequence 3(*a*)–3(*e*)–3(*a*)–3(*b*)–3(*a*)–3(*e*)–3(*a*), with the 3(*b*) section representing that in which sustained oscillations will be seen experimentally.

In the above scenario, there is little interaction between the multiple-stationary-state and Hopf phenomena. Closer to the line Δ, however, new patterns arising from such interactions become important. If the upper Hopf point moves into the upper region of stationary-state hysteresis, a phase portrait of the form in figure 3*f* appears. There are three stationary points. The lowest is a stable sink, the middle a saddle and the upper an unstable source. The upper, unstable state is surrounded by a stable limit cycle that lies completely above the separatrix of the saddle. Again we have coexisting oscillatory and steady states, but here the oscillations are about a different state.

In both cases considered so far, the limit cycle survives across the whole range for which the uppermost state is unstable. Increasing the residence time we thus see first an ignition as the system jumps from the lower branch to the upper at the end of the first region of multiplicity. Moving then along the upper branch, steady behaviour gives way to oscillations for a short range of residence time, before the upper state become stable again. We then stay on this upper state until the high τ_{res} extinction point. If we now reduce τ_{res}, we ultimately encounter the ignition point and jump back towards the upper state. If the latter is stable it will be attained, but if it is

unstable we shall move onto the stable limit cycle, another hard excitation into oscillations but here associated with stationary-state multiplicity rather than a subcritical Hopf bifurcation.

More significant, however, is the change in response to that shown in figure 2*h*. Now the locus of stable limit cycles around the uppermost branch is broken. For intermediate residence times between the Hopf points the limit cycles appear to merge with the saddle point branch and disappear. This is reasonable explanation of what does happen: the limit cycle solutions disappear through homoclinic orbit formation. This is an important feature for oscillatory solutions with multiple stationary states and is discussed in some detail below. For now, we can simply recognize the consequences.

A new phase portrait has been encountered: between the homoclinic bifurcations we have three stationary states, the lowest is stable, the middle a saddle and the uppermost as shown in figure 3*g*. There are no limit cycles. All initial points eventually approach the single stable state, that at low extents of reaction on the bottom branch of the hysteresis loop. Thus if we increase the residence time from below the first Hopf point we begin on the upper branch, develop into small oscillations about this state as it becomes unstable and then encounter an early extinction, not at the end saddle-node point but at the first homoclinic bifurcation. We then stay on the lower branch even though a stable limit cycle appears and then the upper state regains stability at higher residence times.

Figure 2*i*, *j* shows two possible forms for the stationary-state bifurcation diagram in region 8. Both would give rise to the same experimental observations but different in the exact fate of the unstable limit cycle. There are two Hopf points, one on the upper branch of the mushroom, the other from the low stationary state near the upper region of hysteresis. The former of these is a supercritical Hopf point and hence gives birth to a stable limit cycle. The saddle-node bifurcation at which the lowest middle branches reappear now occurs inside the large, stable limit cycle. The phase portrait here is as in figure 3*h*, with two unstable sources and a saddle inside one stable limit cycle. This change in phase portrait would have no effect on the experimental observation that would be still a large-amplitude oscillation. Increasing τ_{res} further, the lower stationary point undergoes a subcritical Hopf bifurcation from which an unstable limit cycle emerges as the lower state becomes stable. The phase portrait is now as in figure 3*i*.

The ultimate fate of the large amplitude oscillations is to disappear by merging with the unstable limit cycle created at the upper Hopf bifurcation. This occurs in figure 2*i*, *j* in each case after the uppermost stationary state has undergone a saddle-node bifurcation. We thus get a 'hard extinction' from the oscillations to the low-extent-of-reaction-state. The only difference between these two scenarios is that the unstable limit cycle may itself disappear over some range of residence time, involving a pair of homoclinic orbit bifurcations. Between these, there is another phase portrait, figure 3*j*, but no change in the experimental consequences.

(*e*) *Regions 4 and 7: homoclinic orbits*

The final two regions, 4 and 7, of the parameter plane lie below the curve Δ. These parameter combinations allow multiple stationary states – isolas and mushrooms, respectively – but only one Hopf bifurcation point. Both regions are also subdivided by the broken line emerging from $\kappa_2 = \frac{9}{256}$ with $\beta_0 = 0$ and terminating at the junction of Δ and H at $\kappa_2 = \frac{9}{2}(2-\sqrt{3})^3$, $\beta_0 = \frac{1}{2}(3^{\frac{3}{2}}-5)$.

In region 4(i), the stationary-state locus has the form of figure 2*k*. There is a Hopf bifurcation along the upper branch of the isola: the upper branch is stable at low residence times and unstable above the Hopf point. The Hopf bifurcation in this case is subcritical, so an unstable limit cycle emerges and grows as the residence time decreases. A new phase portrait is found, figure 3*k*, with a stable stationary point, a saddle and a second stable state that is surrounded by an unstable limit cycle. If the system can be persuaded onto the upper shore of the isola at low residence times, a stable steady state can be attained. However, extinction from this upper state occurs when the residence time reaches the Hopf point, well before the right-hand saddle-node bifurcation. The unstable limit cycle has little physical effect, and terminates in a homoclinic orbit.

In region 4(ii), the Hopf bifurcation has become supercritical, figure 2*l*. As we move along the upper shore of the isola, the high-extent-of-conversion stationary state loses local stability and small-amplitude oscillations about that state emerge. The amplitude grows as τ_{res} is increased further until the oscillations are extinguished. Close inspection reveals that the stable limit cycle itself does not take part in the homoclinic bifurcation. Just before the stable limit cycle disappears, an unstable cycle is born at a homoclinic point, and the unstable cycle then annihilates the stable one. This creates a phase portrait of the form in figure 3*l* where the upper, unstable state is surrounded by a stable limit cycle and both are surrounded by an unstable cycle.

Whether the stable limit cycle itself becomes homoclinic, or whether the above scenario always holds has little influence on the corresponding experimental observations. Either way, the limit cycle undergoes hard extinction and the system moves to the lower stationary state before the right-hand saddle-node bifurcation is reached. Clearly, however, some attention should be paid to the mechanism of the homoclinic bifurcation. This is most easily understood by recognizing that it is not the limit cycle but the saddle point that 'becomes homoclinic'. Homoclinicity is achieved when one inset and one outset from the saddle actually join up to form a closed loop. This sequence is illustrated in figure 5, accompanying a variation in some parameter such as the residence time. In figure 5*a*, the inset and outset do not meet: the outset curls inside the inset, tending to the stable stationary point also in the plane. For figure 5*b*, homoclinicity has been achieved. The closed loop thus formed survives as the parameter is varied further, but detaches itself from the saddle while still surrounding the stable stationary point, figure 5*c*. The inset and outset avoid each other again, but their relative positions have been reversed. This sequence has described the formation of an unstable homoclinic loop and limit cycles, but by reversing the stability of the other stationary point and the direction of the arrows on the inset and outset a stable cycle can be formed in exactly the same way.

An important, and experimentally observable, feature of the death of a stable limit cycle by homoclinic-orbit formation is that the period of the corresponding oscillations lengthens dramatically. As the homoclinic loop actually has a stationary point (the saddle) on it, it takes infinite time for a complete orbit. Just before the loop is formed, the oscillatory period lengthens, tending to infinity logarithmically with the distance of the appropriate parameter from the homoclinic value.

The basic form of figures 2*k*, *l* can be found even for systems with no autocatalyst in the inflow, $\beta_0 = 0$. For higher values of β_0 away from the axis in figure 1, other isola plus single Hopf forms have been conjectured, shown in figure 2*m*–*p*, their existence inferred in part from the 'consistency' arguments of Gray & Roberts (1988*a*–*d*).

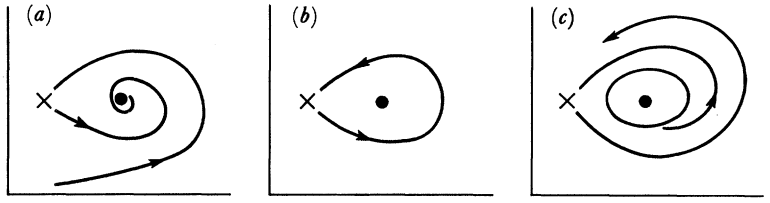

Figure 5. The creation of an unstable limit cycle via a homoclinic-orbit bifurcation from a saddle point.

Some of the extra boundaries which further subdivide the regions have been computed (W. W. Farr, personal communication 1989): the subregions are generally very small indeed in the parameter plane, so they are unlikely to be observed experimentally, at least not by accident. Associated with these extra bifurcation curves are two new phase portraits (figure 3*m*, *n*).

There is a similar wide variety of mushroom patterns with a single Hopf point in region 7. The simplest situations are those of a subcritical or a supercritical point with the emerging limit cycle itself forming a homoclinic orbit, regions 7(i) and (ii), respectively. Of these, the case with a supercritical Hopf bifurcation leading to the formation of a stable limit cycle as the residence time increases is the one of greatest experimental significance. Two slight variations on this theme are shown in figure 2*r*, *s*. In the first of these, the stable limit cycle forms a homoclinic orbit at some point along the saddle branch. If we start an experiment at some residence time below the Hopf point the system may attain a stationary state of high conversion on the top of the mushroom. As τ_{res} is increased, oscillation sets in as we pass the Hopf point. As the homoclinic point is approached, so the period of the oscillation increases as discussed above. Oscillatory reaction ceases at the homoclinic point and the system moves to the steady, low extent state. If we now decrease the residence time, we stay on the lower state past the homoclinic point, so there is hysteresis between the steady reaction and oscillation.

In figure 2*s*, however, the homoclinic orbit is formed not by a simple saddle, but by the saddle-node point at which the middle and lower branches re-emerge. There are two experimentally observable differences consequent on this change in the nature of the homoclinicity. First, the rate at which the period lengthens as this bifurcation is approached is no longer logarithmic, but is given by the inverse of the square root of the distance from the bifurcation. Secondly, there will be no hysteresis as τ_{res} is increased or decreased. The onset of oscillations as the residence time is decreased is a hard excitation. The facts will be pertinent to our discussion of the hydrogen–oxygen reaction in the next section.

Finally, the additional bifurcation diagrams appropriate to region 7 are collected in figure 2*q*, *t*, *u*. These involve no new phase portraits.

4. Discussion

(*a*) *Other model schemes*

Figures 2 and 3 present the 21 bifurcation diagrams and 14 phase portraits relevant to the present cubic autocatalysis model. Similar numbers have been observed or predicted for other two-variable chemical models including the classic first-order exothermic reaction in a CSTR (Uppal *et al.* 1974, 1976; Vaganov *et al.* 1978; Jorgensen *et al.* 1984) and a selection of isothermal schemes (Guckenheimer

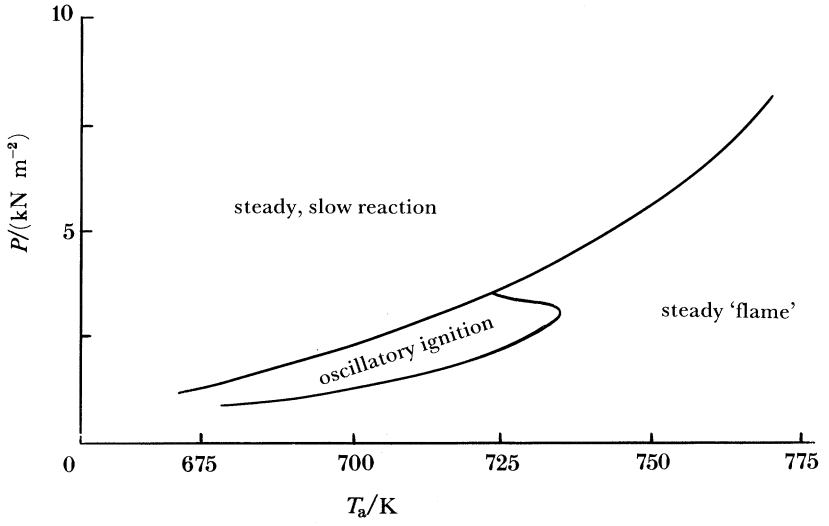

Figure 6. The $p-T_a$ ignition diagram for a stoichiometric mixture $2H_2+O_2$ in a CSTR: mean residence time = 4 s. (From Griffiths *et al.* (1990).)

1986; Gray & Roberts 1988*a–d*). We can thus feel confident that studies of simple schemes reveal generic patterns of behaviour, applicable to a much wider class, and to real systems in particular. With this confidence, we now use the results of the previous section to interpret the responses observed in the spontaneous oxidation of hydrogen in a CSTR. Although the latter involves many different chemical species and reaction steps, and the underlying rate law is closer to quadratic autocatalysis with an extra inhibition step than to the present cubic model, we shall see that this system has much behaviour that can be identified with two-variable dynamics.

(*b*) *The hydrogen–oxygen reaction in a* CSTR

The behaviour of equimolar or stoichiometric mixtures of hydrogen and oxygen (H_2+O_2 and $2H_2+O_2$) at pressures between 1–10 kN m^{-2} and temperatures in the range 700–800 K in a CSTR with mean residence times of 2–10 s has been determined in a series of experiments (Gray *et al.* 1984*a*, *b*, 1987; Gray & Scott 1985*b*). Typically, the mixture composition, pressure and residence time are fixed during a given experiment and the ambient temperature T_a varied. Figure 6 shows an ignition diagram appropriate to a fixed residence time and composition, obtained by repeated experiments at different total pressures. At low ambient temperatures, a slow steady reaction is observed, with low extents of hydrogen or oxygen consumption (less than *ca.* 5%) and only small extents of self-heating by the exothermic reaction ($\Delta T < 10$ K). As the ambient temperature is increased, the system crosses an 'ignition limit'. Above the limit, the mode of reaction is 'oscillatory ignition': there is hard excitation to large amplitude, repetitive explosions with a period longer than the mean residence time. As T_a is further increased, the amplitude and period decrease: figure 7*a* shows a sequence of typical oscillatory traces and curve (*a*) of figure 8 plots the variation of period with ambient temperature. Eventually, the oscillatory amplitude decreases to zero and a stable stationary state emerges (a steady 'flame'). If T_a is decreased again, oscillatory behaviour resumes at the same point at which it disappeared and grows smoothly from zero amplitude.

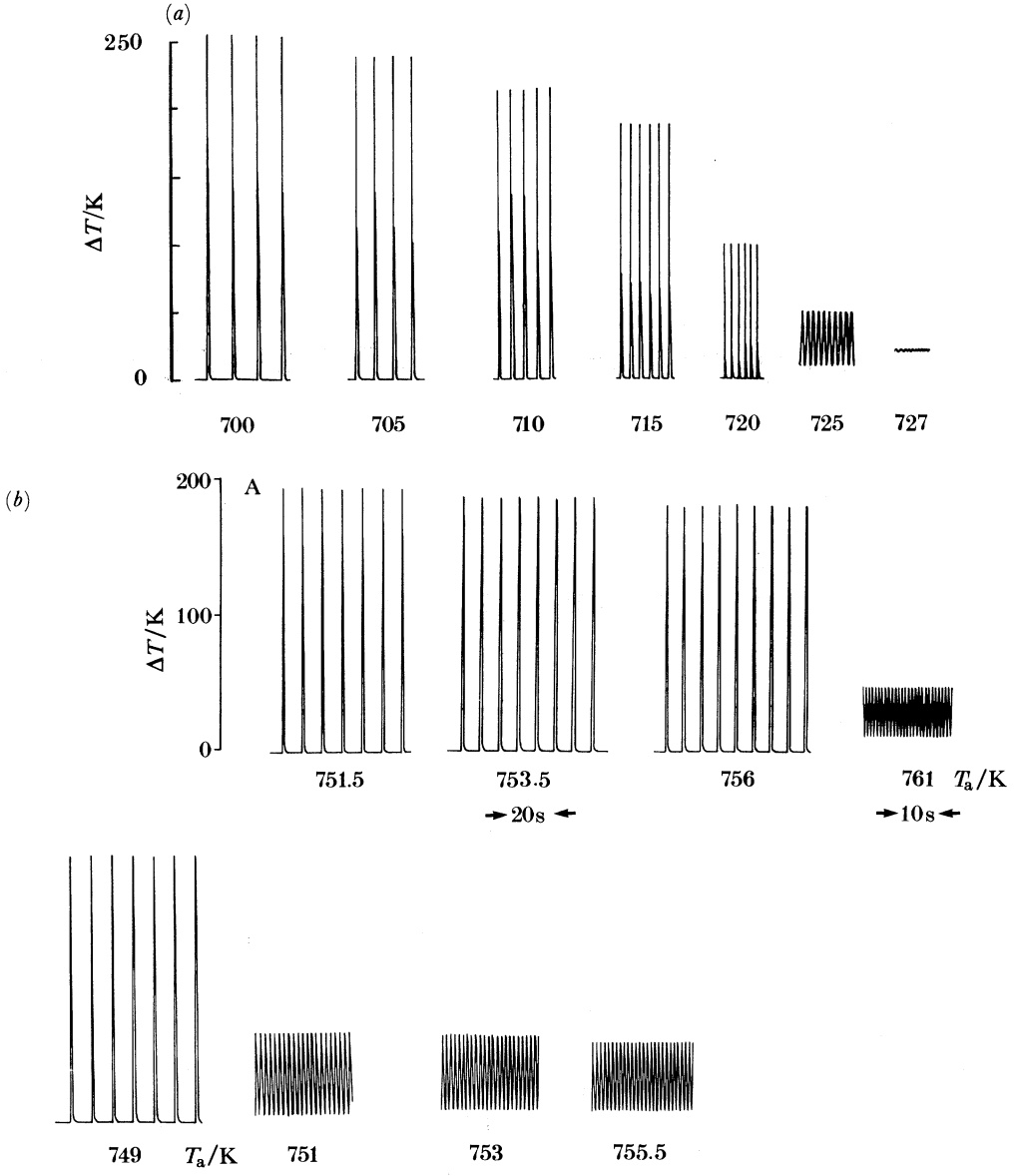

Figure 7. Variation in oscillatory amplitude during ignition in stoichiometric $2H_2+O_2$ mixtures: (*a*) $t_{res} = 8$ s; (*b*) $t_{res} = 2$ s, showing discontinuous change in amplitude and birhythmicity.

The disappearance of oscillations at low T_a coincides with the location of the ignition limit: there is hard extinction, but no hysteresis. The period lengthens dramatically, growing as $(T_a - T_{a,cr})^{-\frac{1}{2}}$, where $T_{a,cr}$ is the value of the ambient temperature at the ignition limit.

At higher total pressures, the system may apparently jump straight to the upper steady-flame state as it crosses the limit. Also, for slightly different residence times, the variation of oscillatory waveform with ambient temperature is not smooth: instead there are jumps between large and small amplitude ignitions and birhythmicity as shown in figure 7*b* and curve (*b*) in figure 8.

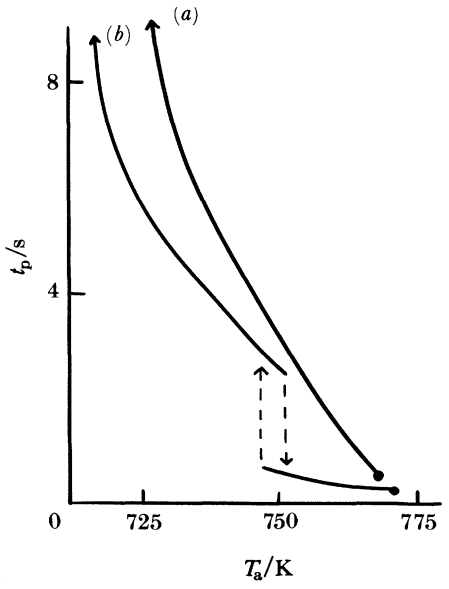

Figure 8. Variation of oscillatory period with ambient temperature for sequences in figure 7*a*, *b*.

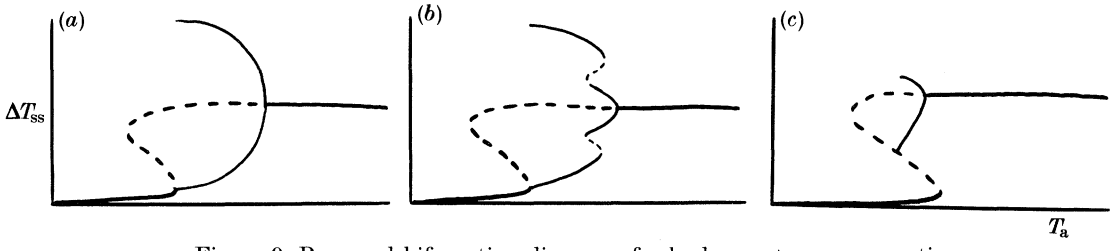

Figure 9. Proposed bifurcation diagrams for hydrogen + oxygen reaction.

Figure 9 shows two bifurcation loci drawn from experience gained through the cubic autocatalytic model, which would reproduce the experimental observations just described. For the first scenario, we may conjecture a hysteresis loop, figure 9*a*, with an ignition saddle-node bifurcation on increasing T_a. Above the ignition point, the upper state is unstable and surrounded by a large-amplitude limit cycle. This cycle is formed from a homoclinic orbit from the saddle-node point: there will be no hysteresis and the period will lengthen, as observed experimentally. As T_a is increased, the limit cycle becomes smaller, and disappears at a supercritical Hopf bifurcation. For higher ambient temperatures the upper stationary state is stable.

For figure 9*b*, many of the above features remain, but the locus of limit cycle solutions has become folded back on itself for some range below the Hopf point. This gives a region with three limit cycles, two of which are stable and these have large and small amplitudes, respectively. Such an arrangement will give rise to birhythmicity, and can be simply unfolded to yield figure 9*a* by varying a parameter such as the residence time.

In figure 9*c*, the Hopf point has moved to an ambient temperature below that of the ignition saddle-node bifurcation. For such a diagram, the system would jump to a stable upper state. However, we might still hope to find oscillations, by reducing

T_a below the ignition limit once we have moved on to the upper branch. The oscillations might not survive for a wide range of ambient temperature, as homoclinic orbits are typically formed rapidly in regions of multiple stationary states. We may also predict that some hysteresis should be detectable at the limit for these higher pressures and that if oscillations can be observed, their period will lengthen on approaching the homoclinic point in a different way from that observed previously.

Conclusions

1. A very basic chemical scheme for autocatalytic reaction leads to very rich patterns of behaviour in the simplest of open systems, the CSTR. The reaction sequence is simple: $A + 2B \rightarrow 3B$ with rate proportional to ab^2, followed by $B \rightarrow C$ with rate proportional to b. There are only two chemical components A and B and reaction is isothermal.

2. This isothermal scheme has many resemblances to the first-order exothermic reaction system which depends on (exponential) thermal feedback, and appears to display an equal number of different patterns of behaviour. It may fairly be called archetypal.

3. Reversibility is not necessary for oscillatory behaviour but it can readily be accommodated. It does not increase the variety of behaviour.

4. The scheme has many illuminating applications. For example, nested limit cycles can be generated that describe 'birhythmic' behaviour identical to that recently found in the oxygen–hydrogen reaction.

Appendix

The stationary states for the cubic autocatalysis model are given by equations (10) and (11). Once a given stationary-state solution has been located, its local stability to infinitesimal perturbations $(\Delta\alpha, \Delta\beta)$ can be determined from the linearized equations

$$\frac{\mathrm{d}}{\mathrm{d}\tau}\begin{bmatrix}\Delta\alpha\\ \Delta\beta\end{bmatrix} = J\begin{bmatrix}\Delta\alpha\\ \Delta\beta\end{bmatrix}, \tag{A 1}$$

where J is the jacobian matrix

$$J = \begin{bmatrix}\partial(\mathrm{d}\alpha/\mathrm{d}\tau)/\partial\alpha & \partial(\mathrm{d}\alpha/\mathrm{d}\tau)/\partial\beta\\ \partial(\mathrm{d}\beta/\mathrm{d}\tau)/\partial\alpha & \partial(\mathrm{d}\beta/\mathrm{d}\tau)/\partial\beta\end{bmatrix}. \tag{A 2}$$

For the present model, the jacobian has the particular form

$$J = \begin{bmatrix}-\tau_{\mathrm{res}}^{-1} - \beta_{\mathrm{ss}}^2 & -2\alpha_{\mathrm{ss}}\beta_{\mathrm{ss}}\\ \beta_{\mathrm{ss}}^2 & -\tau_{\mathrm{res}}^{-1} + 2\alpha_{\mathrm{ss}}\beta_{\mathrm{ss}} - \kappa_2\end{bmatrix}. \tag{A 3}$$

The perturbations decay or grow as the sum of exponential terms in $\lambda_1\tau$ and $\lambda_2\tau$, where $\lambda_{1,2}$ are the eigenvalues of the jacobian. These, in turn are given by the quadratic equation

$$\lambda^2 - \mathrm{tr}\,(J)\,\lambda + \det(J) = 0, \tag{A 4}$$

where $\mathrm{tr}\,(J)$ and $\det(J)$ are the trace and determinant of J.

For a two-variable system, the condition for Hopf bifurcation can be expressed simply as

$$\mathrm{tr}\,(J) = 0 \tag{A 5}$$

subject to the extra conditions

$$\det(J) > 0 \quad \text{and} \quad \mathrm{d}\,\mathrm{tr}(J)/\mathrm{d}\tau_{\mathrm{res}} \neq 0 \tag{A 6}$$

when (A 5) is satisfied.

Saddle-node bifurcation can similarly be conveniently identified by the condition

$$\det(J) = 0, \tag{A 7}$$

or, in terms of the stationary-state equation (11), by

$$F_\alpha = 0, \tag{A 8}$$

where the subscript denotes differentiation with respect to the dimensionless concentration of A.

The various loci in figure 1 correspond to *degenerate bifurcations*. Two types of stationary-state degeneracy occur for this model:

$$\text{hysteresis variety} \quad F = F_\alpha = F_{\alpha\alpha} = 0; \tag{A 9}$$

$$\text{isola variety} \quad F = F_\alpha = F_{\tau_{\mathrm{res}}} = 0. \tag{A 10}$$

The first of these conditions give the line $\beta_0 = \frac{1}{8}$ in figure 1: the second is given by

$$\kappa_2 = \tfrac{1}{32}\{1 + 20\beta_0 - 8\beta_0^2 \pm (1 - 8\beta_0)^{\frac{3}{2}}\}, \tag{A 11}$$

which has two branches, forming the cusp in figure 1. The two types of degeneracy occur together when $F = F_\alpha = F_{\alpha\alpha} = F_{\tau_{\mathrm{res}}} = 0$ at $\beta_0 = \frac{1}{8}, \kappa_2 = 3^3/4^4$.

The line H is a locus of degenerate Hopf points determined by the condition

$$F = \mathrm{tr}(J) = \mathrm{d}\,\mathrm{tr}(J)/\mathrm{d}\tau_{\mathrm{res}} = 0, \tag{A 12}$$

which governs where two Hopf points merge. It is only valid for $\beta_0 > \frac{1}{2}(3^{\frac{3}{2}} - 5)$. The curve Δ is the so-called double-zero-eigenvalue degeneracy

$$F = \mathrm{tr}(J) = \det(J) = 0, \tag{A 13}$$

where a Hopf point coincides with a saddle-node bifurcation. This locus is parametrized by

$$\beta_0 = x(1-2x), \quad \kappa_2 = 4x^2(1-x)^4$$

with $0 \leqslant x \leqslant \frac{1}{2}$.

The broken curves in figure 1 are related to the changing stability of the emerging limit cycle at a Hopf bifurcation.

We are grateful to Dr J. F. Griffiths and Mr B. Johnson of Leeds, and to Professor B. F. Gray and Dr M. J. Roberts of Sydney for their generous advice and cooperation. We also thank NATO, the SERC and Gonville and Caius College for support.

References

Amundson, N. R. 1955 *AIChE J.* **1**, 513–520.

Amundson, N. R. & Aris, R. 1958 *Chem. Engng Sci.* **7**, 121–131.

Aris, R., Gray, P. & Scott, S. K. 1988 *Chem. Engng Sci.* **43**, 207–211.

Cook, G. B., Gray, P., Knapp, D. & Scott, S. K. 1989 *J. phys. Chem.* **93**, 2749–2755.

Farr, W. W. & Scott, S. K. 1988 *Chem. Engng Sci.* **43**, 1708–1710.

Gray, B. F. & Roberts, M. J. 1988*a* *Proc. R. Soc. Lond.* A **416**, 361–389.

Gray, B. F. & Roberts, M. J. 1988*b* *Proc. R. Soc. Lond.* A **416**, 391–402.

Gray, B. F. & Roberts, M. J. 1988*c* *Proc. R. Soc. Lond.* A **416**, 403–424.

Gray, B. F. & Roberts, M. J. 1988*d* *Proc. R. Soc. Lond.* A **416**, 425–441.

Gray, P. & Scott, S. K. 1983 *Chem. Engng Sci.* **38**, 29–43.

Gray, P. & Scott, S. K. 1984 *Chem. Engng Sci.* **39**, 1087–1097.

Gray, P. & Scott, S. K. 1985*a* *J. phys. Chem.* **89**, 22–32.

Gray, P. & Scott, S. K. 1985*b* In *Oscillations and traveling waves in chemical systems* (ed. R. J. Field & M. Burger), ch. 14, pp. 493–528. New York: Wiley.

Gray, P. & Scott, S. K. 1989 *Chemical oscillations and instabilities.* Oxford University Press.

Gray, P., Griffiths, J. F. & Scott, S. K. 1984*a* *Proc. R. Soc. Lond.* A **394**, 243–258.

Gray, P., Griffiths, J. F. & Scott, S. K. 1984*b* In *20th Symp.* (*Int.*) *Combust.*, pp. 1809–1815. Pittsburgh: Combustion Institute.

Gray, P., Griffiths, J. F., Pappin, A. J. & Scott, S. K. 1987 *In Complex chemical reaction systems* (ed. J. Warnatz & W. Jäger), pp. 150–159. Berlin: Springer-Verlag.

Griffiths, J. F., Johnson, B. J. & Scott, S. K. 1990 (In preparation.)

Guckenheimer, J. 1986 *Physica.* D **20**, 1–20.

Jorgensen, D., Farr, W. W. & Aris, R. 1984 *Chem. Engng Sci.* **39**, 1741–1752.

Kaas-Petersen, C., McGarry, J. K. & Scott, S. K. 1989 *J. chem. Soc. Faraday Trans.* II **83**, 1831–1835.

Sal'nikov, I. Ye. 1948 *Dokl. Akad. Nauk. SSSR* **60**, 405–408.

Uppal, A., Ray, R. W. H. & Poore, A. B. 1974 *Chem. Engng Sci.* **29**, 967–985.

Uppal, A., Ray, R. W. H. & Poore, A. B. 1976 *Chem. Engng Sci.* **31**, 205–214.

Vaganov, D. A., Samoilenko, N. G. & Abramov, V. G. 1978 *Chem. Engng Sci.* **33**, 1133–1143.

Zel'dovich, Ya. B. 1941 *Zh. tekh. Fiz.* **11**, 493–500.

Zel'dovich, Ya. B. & Zysin, Y. A. 1941 *Zh. tekh. Fiz.* **11**, 501–508.

PHILOSOPHICAL TRANSACTIONS OF THE ROYAL SOCIETY A MATHEMATICAL, PHYSICAL & ENGINEERING SCIENCES